Article

Ferrous Binding to the Multicopper Oxidases *Saccharomyces cerevisiae* Fet3p and Human Ceruloplasmin: Contributions to Ferroxidase Activity

Liliana Quintanar, Mark Gebhard, Tzu-Pin Wang, Daniel J. Kosman, and Edward I. Solomon

J. Am. Chem. Soc., **2004**, 126 (21), 6579-6589• DOI: 10.1021/ja049220t • Publication Date (Web): 07 May 2004

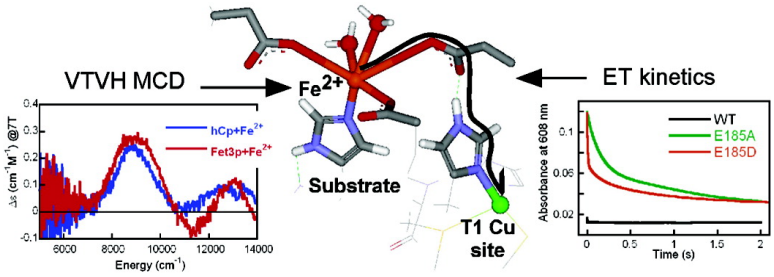

More About This Article

Additional resources and features associated with this article are available within the HTML version:

- Supporting Information
- Links to the 5 articles that cite this article, as of the time of this article download
- Access to high resolution figures
- Links to articles and content related to this article
- Copyright permission to reproduce figures and/or text from this article

View the Full Text HTML

J|A|C|S
ARTICLES
Published on Web 05/07/2004

Ferrous Binding to the Multicopper Oxidases *Saccharomyces cerevisiae* Fet3p and Human Ceruloplasmin: Contributions to Ferroxidase Activity

Liliana Quintanar,[†] Mark Gebhard,[†] Tzu-Pin Wang,[‡] Daniel J. Kosman,*[,‡] and Edward I. Solomon*[,†]

Contribution from the Department of Chemistry, Stanford University, Stanford, California 94305-5080, and Department of Biochemistry, School of Medicine and Biomedical Sciences, State University of New York, Buffalo, New York 14214

Received February 12, 2004; E-mail: edward.solomon@stanford.edu

Abstract: The multicopper oxidases are a family of enzymes that couple the reduction of O_2 to H_2O with the oxidation of a range of substrates. *Saccharomyces cerevisiae* Fet3p and human ceruloplasmin (hCp) are members of this family that exhibit ferroxidase activity. Their high specificity for Fe(II) has been attributed to the existence of a binding site for iron. In this study, mutations at the E185 and Y354 residues, which are putative ligands for iron in Fet3p, have been generated and characterized. The effects of these mutations on the electronic structure of the T1 Cu site have been assessed, and the reactivities of this site toward 1,4-hydroquinone (a weak binding substrate) and Fe(II) have been evaluated and interpreted in terms of the semiclassical Marcus theory for electron transfer. The electronic and geometric structure of the Fe(II) substrate bound to Fet3p and hCp has been studied for the first time, using variable-temperature variable field magnetic circular dichroism (VTVH MCD) spectroscopy. The iron binding sites in Fet3p and hCp appear to be very similar in nature, and their contributions to the ferroxidase activity of these proteins have been analyzed. It is found that these iron binding sites play a major role in tuning the reduction potential of iron to provide a large driving force for the ferroxidase reaction, while still supporting the delivery of the Fe(III) product to the acceptor protein. Finally, the analysis of possible electron-transfer (ET) pathways from the protein-bound Fe(II) to the T1 Cu site indicates that the E185 residue not only plays a role in iron binding, but also provides the dominant ET pathway to the T1 Cu site.

Introduction

The multicopper oxidases are a family of enzymes that couple the one-electron oxidation of four substrate equivalents with the four electron reduction of O_2 to H_2O.[1] The catalytic motif in these proteins includes at least four Cu atoms that are classified into three types of sites according to their spectroscopic properties: type 1 (T1) or blue Cu, type 2 (T2) or normal Cu, and type 3 (T3) or coupled binuclear Cu sites. The absorption spectrum of the T1 Cu site is characterized by an intense Cys-S to Cu(II) charge-transfer (CT) band at about 600 nm, while its electron paramagnetic resonance (EPR) spectrum exhibits a narrow parallel hyperfine splitting ($A_{\|} = (40-95) \times 10^{-4}$ cm^{-1}). The T2 or normal Cu site is characterized by the lack of strong absorption features, and its EPR spectrum exhibits a normal, large parallel hyperfine splitting ($A_{\|} = (140-200) \times 10^{-4}$ cm^{-1}). The T3 site is composed of two Cu(II) atoms antiferromagnetically coupled through a hydroxide bridge. It is characterized by an intense CT band at about 330 nm (originating from the bridging hydroxide) and the lack of an EPR signal, due to the antiferromagnetic coupling. The T2 and T3 sites form a trinuclear Cu cluster, which is the site of oxygen reduction,[2−5] while the main functional role of the T1 Cu site is to shuttle electrons from the substrate to the trinuclear Cu site.

The multicopper oxidases are present in several organisms.[1] They are important for lignin formation in plants (plant laccases),[6,7] pigment formation, lignin degradation, and detoxification processes in fungi (fungal laccases),[8−11] iron metabolism in yeast (Fet3p)[12,13] and mammals (hCp[14−19] and hephaestin[20,21]),

[†] Stanford University.
[‡] State University of New York.

(1) Solomon, E. I.; Sundaram, U. M.; Machonkin, T. E. *Chem. Rev.* **1996**, *96*, 2563−2605.
(2) Allendorf, M. D.; Spira, D. J.; Solomon, E. I. *Proc. Natl. Acad. Sci. U.S.A.* **1985**, *82*, 3063.
(3) Spira-Solomon, D. J.; Allendorf, M. D.; Solomon, E. I. *J. Am. Chem. Soc.* **1986**, *108*, 5318.
(4) Cole, J. L.; Tan, G. O.; Yang, E. K.; Hodgson, K. O.; Solomon, E. I. *J. Am. Chem. Soc.* **1990**, *112*, 2243−2249.
(5) Messerschmidt, A.; Ladenstein, R.; Huber, R.; Bolognesi, M.; Avigliano, L.; Petruzzelli, R.; Rossi, A.; Finazzi-Agro, A. *J. Mol. Biol.* **1992**, *224*, 179−205.
(6) Oshima, R.; Yamauchi, Y.; Watanabe, C.; Kumanotani, J. *J. Org. Chem.* **1985**, *50*, 2613−2621.
(7) Sterjiades, R.; Dean, J. F. D.; Eriksson, K.-E. L. *Plant Physiol.* **1992**, *99*, 1162−1168.
(8) Ander, P.; Eriksson, K.-E. *Arch. Microbiol.* **1976**, *109*, 1−8.
(9) Clutterbuck, A. J. *J. Gen. Microbiol.* **1972**, *70*, 423−435.
(10) Thurston, C. F. *Microbiology* **1994**, *140*, 19−26.
(11) Claus, H. *Arch. Microbiol.* **2003**, *179*, 145−150.
(12) Askwith, C.; Eide, D.; VanHo, A.; Bernard, P. S.; Li, L.; Davis-Kaplan, S.; Sipe, D. M.; Kaplan, J. *Cell* **1994**, *76*, 403−410.
(13) de Silva, D.; Askwith, C. C.; Eide, D.; Kaplan, J. *J. Biol. Chem.* **1995**, *270*, 1098−1101.

copper homeostasis in bacteria (CueO),[22−25] and manganese oxidation by bacterial spores (MnxG).[26−28] Therefore, the physiological substrates of the multicopper oxidases vary from organic compounds to metal ions such as Fe(II),[29,30] and possibly Cu(I)[31] and Mn(II).

Some members of the family, like the fungal laccases, are able to oxidize a wide variety of aromatic compounds very efficiently.[1,32] In contrast, Fet3p and hCp exhibit slow oxidation of phenolic compounds and a strong specificity for Fe(II), indicating that Fe(II) is their physiological substrate.[33] Along with the iron permease Ftr1p, Fet3p is part of a high-affinity Fe uptake system in *Saccharomyces cerevisiae*;[12,34−36] this system is activated under low iron conditions (K_M is 0.15 μM).[37,38] Fet3p contains one transmembrane domain, and the Fe(III) product of its ferroxidase reaction is transferred to Ftr1p for transport across the membrane.[39] In humans, hCp has been proposed to play a role in iron metabolism.[35,40] Fe(II) is oxidized by hCp, and the Fe(III) product is delivered to transferrin (Tf), a soluble Fe(III)-carrier in blood plasma. In both yeast and humans, the ferroxidase activity of these multicopper oxidases and their high affinity for Fe(II) are critical for iron metabolism.[41]

Several multicopper oxidases have been structurally characterized.[5,42−53] Crystal structures exist for hCp in the resting oxidized form,[44] and with bound metals,[45] organic substrates, and azide.[43] hCp is the most complex of the multicopper oxidases, containing one trinuclear Cu cluster and 3 T1 Cu sites, one of which is permanently reduced.[54] The other two T1 Cu sites are redox-active and competent to participate in the ferroxidase reaction.[55] The crystal structures on the Co and Cu bound forms of hCp[45] have identified one divalent metal ion binding site ~9 Å directly above each of the two redox-active[54,55] T1 Cu sites. In domain 6, the ligands for the divalent metal ion are E272, D1025, E935, and H940; a similar scenario is found in domain 4, where E971, D684, E597, and H602 are the putative ligating residues. A site-directed mutagenesis study of hCp[56] has shown that the double mutant E935A/H940A exhibits reduced ferroxidase activity (50%), confirming the involvement of these residues in iron binding.

In the absence of a crystal structure for Fet3p, several sequence homology studies have attempted to identify the putative ligands for a ferrous binding site in this protein.[57−59] A homology modeling study based on the crystal structure of *Cucurbita pepo medullosa* ascorbate oxidase[58] identified three putative Fe(II) binding residues, E185, D409, and Y354, all of them conserved in the sequences of *Candida albicans* Fet3p and its homologue in *Schizosaccharomyces pombe* (Fio1p). Mutation of E185 to Ala yielded a significant increase in K_M for Fe(II) under turnover conditions,[59,60] and the E185A mutant showed no iron uptake in vivo,[59] indicating that this residue may play an important role in Fe(II) binding. Mutations of the Y354 residue have yielded modest decreases in ferroxidase activity[59,60] that have been ascribed to the role of this residue in stabilizing the Fe(II) complex.[59] The mutation of D409 to Ala has only been tested in vivo, yielding a very modest increase in the K_M associated with iron uptake.[61] Finally, a second structural model of Fet3p has been constructed on the basis of the crystal structure of *Coprinus cinereus* laccase, positioning the E185 and Y354 residues within 15 Å of the T1 Cu site and identifying D278 as another putative ligand for Fe(II).[59] D278 is a residue conserved in *Schizosaccharomyces pombe* Fio1p,

(14) Ragan, H. A.; Nacht, S.; Lee, G. R.; Bishop, C. R.; Cartwright, G. E. *Am. J. Physiol.* **1969**, *217*, 1320−1323.
(15) Osaki, S.; Johnson, D. A.; Frieden, E. *J. Biol. Chem.* **1966**, *241*, 2746−2751.
(16) Okamoto, N.; Wada, S.; Oga, T.; Kawabata, Y.; Baba, Y.; Habu, D.; Takeda, Z.; Wada, Y. *Hum. Genet.* **1996**, *97*, 755−758.
(17) Harris, Z. L.; Takahashi, Y.; Miyajima, H.; Serizawa, M.; MacGillivray, R. T. A.; Gitlin, J. D. *Proc. Natl. Acad. Sci. U.S.A.* **1995**, *92*, 2539−2543.
(18) Harris, Z. L.; Durley, A. P.; Man, T. K.; Gitlin, J. D. *Proc. Natl. Acad. Sci. U.S.A.* **1999**, *96*, 10812−10817.
(19) Hellman, N. E.; Gitlin, J. D. *Annu. Rev. Nutr.* **2002**, *22*, 439−458.
(20) Vulpe, C. D.; Kuo, Y. M.; Murphy, T. L.; Cowley, L.; Askwith, C.; Libina, N.; Gitschier, J.; Anderson, G. J. *Nat. Genet.* **1999**, *21*, 195−199.
(21) Li, L.; Vulpe, C. D.; Kaplan, J. *Biochem. J.* **2003**, *375*, 793−798.
(22) Grass, G.; Rensing, C. *Biochem. Biophys. Res. Commun.* **2001**, *286*, 902−908.
(23) Grass, G.; Rensing, C. *J. Bacteriol.* **2001**, *183*, 2145−2147.
(24) Outten, F. W.; Huffman, D. L.; Hale, J. A.; O'Halloran, T. V. *J. Biol. Chem.* **2001**, *276*, 30670−30677.
(25) Rensing, C.; Grass, G. *FEMS Microbiol. Rev.* **2003**, *27*, 197−213.
(26) Waasbergen, L. G. V.; Hildebrand, M.; Tebo, B. M. *J. Bacteriol.* **1996**, *178*, 3517−3530.
(27) Francis, C. A.; Tebo, B. M. *Appl. Environ. Microbiol.* **2002**, *68*, 874−880.
(28) Francis, C. A.; Casciotti, K. L.; Tebo, B. M. *Arch. Microbiol.* **2002**, *178*, 450−456.
(29) de Silva, D.; Davis-Kaplan, S.; Fergestad, J.; Kaplan, J. *J. Biol. Chem.* **1997**, *272*, 14208−14213.
(30) Hassett, R. F.; Yuan, D. S.; Kosman, D. J. *J. Biol. Chem.* **1998**, *273*, 23274−23282.
(31) Stoj, C.; Kosman, D. J. *FEBS Lett.* **2003**, *554*, 422−426.
(32) Xu, F. *J. Biol. Chem.* **1997**, *272*, 924−928.
(33) Machonkin, T. E.; Quintanar, L.; Palmer, A. E.; Hassett, R.; Severance, S.; Kosman, D. J.; Solomon, E. I. *J. Am. Chem. Soc.* **2001**, *123*, 5507−5517.
(34) Askwith, C.; Kaplan, J. *J. Biol. Chem.* **1997**, *272*, 401−405.
(35) Askwith, C.; Kaplan, J. *Trends Biochem. Sci.* **1998**, *23*, 135−138.
(36) Radisky, D.; Kaplan, J. *J. Biol. Chem.* **1999**, *274*, 4481−4484.
(37) Eide, D.; Davis-Kaplan, S.; Jordan, I.; Sipe, D.; Kaplan, J. *J. Biol. Chem.* **1992**, *267*, 20774−20781.
(38) Dancis, A.; Klausner, R. D.; Hinnebusch, A. G.; Barriocanal, J. G. *Mol. Cell. Biol.* **1990**, *10*, 2294−2301.
(39) Stearman, R.; Yuan, D. S.; Yamaguchi-Iwai, Y.; Klausner, R. D.; Dancis, A. *Science* **1996**, *271*, 1552−1557.
(40) Kaplan, J.; O'Halloran, T. V. *Science* **1996**, *271*, 1510−1512.
(41) Kosman, D. J. In *Copper-Containing Proteins*; Valentine, J. S., Gralla, E. B., Eds.; Academic Press Inc: London, UK, 2002; Vol. 60, pp 221−269.
(42) Messerschmidt, A.; Luecke, H.; Huber, R. *J. Mol. Biol.* **1993**, *230*, 997−1014.
(43) Zaitsev, V. N.; Zaitseva, I.; Papiz, M.; Lindley, P. F. *J. Biol. Inorg. Chem.* **1999**, *4*, 579−587.
(44) Zaitseva, I.; Zaitsev, V.; Card, G.; Moshov, K.; Bax, B.; Ralph, A.; Lindley, P. *J. Biol. Inorg. Chem.* **1996**, *1*, 15−23.
(45) Lindley, P. F.; Card, G.; Zaitseva, I.; Zaitsev, V.; Reinhammar, B.; Selin-Lindgren, E.; Yoshida, K. *J. Biol. Inorg. Chem.* **1997**, *2*, 454−463.
(46) Ducros, V.; Brzozowski, A. M.; Wilson, K. S.; Brown, S. H.; Østergaard, P.; Schneider, P.; Yaver, D. S.; Pedersen, A. H.; Davis, G. J. *Nat. Struct. Biol.* **1998**, *5*, 310−316.
(47) Ducros, V.; Brzozowski, A.; Wilson, K.; Ostergaard, P.; Schneider, P.; Svendson, A.; Davies, G. *Acta Crystallogr., Sect. D* **2001**, *57*, 333−336.
(48) Bertrand, T.; Jolivalt, C.; Briozzo, P.; Caminade, E.; Joly, N.; Madzak, C.; Mougin, C. *Biochemistry* **2002**, *41*, 7325−7333.
(49) Hakulinen, N.; Kiiskinen, L.; Kruus, K.; Saloheimo, M.; Paananen, A.; Koivula, A.; Rouvinen, J. *Nat. Struct. Biol.* **2002**, *9*, 601−605.
(50) Piontek, K.; Antorini, M.; Choinowski, T. *J. Biol. Chem.* **2002**, *277*, 37663−37669.
(51) Roberts, S.; Weichsel, A.; Grass, G.; Thakali, K.; Hazzard, J.; Tollin, G.; Rensing, C.; Montfort, W. *Proc. Natl. Acad. Sci. U.S.A.* **2002**, *99*, 2766−2771.
(52) Roberts, S.; Wildner, G.; Grass, G.; Weichsel, A.; Ambrus, A.; Rensing, C.; Montfort, W. *J. Biol. Chem.* **2003**, *278*, 31958−31963.
(53) Enguita, F.; Martins, L.; Henriques, A.; Carrondo, M. *J. Biol. Chem.* **2003**, *278*, 19416−19425.
(54) Machonkin, T. E.; Zhang, H. H.; Hedman, B.; Hodgson, K. O.; Solomon, E. I. *Biochemistry* **1998**, *37*, 9570−9578.
(55) Machonkin, T. E.; Solomon, E. I. *J. Am. Chem. Soc.* **2000**, *122*, 12547−12560.
(56) Brown, M. A.; Stenberg, L. M.; Mauk, A. G. *FEBS Lett.* **2002**, *520*, 8−12.
(57) Murphy, M. E. P.; Lindley, P. F.; Adman, E. T. *Protein Sci.* **1997**, *6*, 761−770.
(58) Bonaccorsi di Patti, M. C.; Pascarella, S.; Catalucci, D.; Calabrese, L. *Protein Eng.* **1999**, *12*, 895−897.
(59) Wang, T.-P.; Quintanar, L.; Severance, S.; Solomon, E. I.; Kosman, D. J. *J. Biol. Inorg. Chem.* **2003**, *8*, 611−620.
(60) Bonaccorsi di Patti, M. C.; Felice, M. R.; Camuti, A. P.; Lania, A.; Musci, G. *FEBS Lett.* **2000**, *472*, 283−286.
(61) Bonaccorsi di Patti, M. C.; Paronetto, M. P.; Dolci, V.; Felice, M. R.; Lania, A.; Musci, G. *FEBS Lett.* **2001**, *508*, 475−478.

and its mutation to Ala increases K_M for Fe(II) in vitro (but to less extent than the E185A mutation), and it has no apparent effect on Fe uptake in vivo.[59]

In this study, we have performed site-directed mutagenesis on Fet3p and have generated soluble forms of E185A, E185D, Y354A, and Y354F Fet3 proteins. We have determined the effects of these mutations on the electronic structure and the reduction potential of the T1 Cu site and have probed the single turnover of the mutated proteins with a bulky organic substrate (1,4-hydroquinone) and with the Fe(II) substrate. Fe(II) binding to Fet3p has been further probed by VTVH MCD spectroscopy, and the site has been compared to the structurally defined iron binding sites in hCp. These studies provide further insight into the nature of the substrate binding site, its role in tuning the substrate for reactivity, and the interactions of the iron binding site with the T1 Cu site.

Experimental Section

All chemicals were reagent grade and used without further purification. Water was purified to a resistivity of 15−17 MΩ cm^{-1} using a Barnstead Nanopure deionizing system. Expression, isolation, and purification of soluble wt, E185A, E185D, Y354A, and Y354F Fet3 proteins were performed as described previously.[59] For isolation of hCp, fresh human plasma was obtained from the Stanford Blood Center, and hCp was purified from the plasma by a rapid one-step method,[62] modified as previously described.[54] hCp samples were used immediately or kept frozen at −80 °C and thawed only once. *Rhus vernicifera* laccase was isolated from acetone powder (Saito and Co., Osaka, Japan) according to published procedures.[63,64] Fet3p and hCp protein concentrations were determined by standard dye-binding Bradford[65] and Biuret[66] assays, respectively. Laccase protein concentration was determined using the extinction coefficient of the absorption band at 280 nm (90 000 M^{-1} cm^{-1}). Copper content was determined spectrophotometrically using 2,2′-biquinoline[67] or by atomic absorption spectroscopy. The concentration of paramagnetic copper was determined from spin quantitation of EPR spectra, using a 1.0 mM $CuSO_4 \cdot 5H_2O$ solution with 2 mM HCl and 2 M $NaClO_4$ standard.[68]

Room-temperature UV−visible absorption spectra were recorded using a Hewlett-Packard HP8452A or an Agilent 8453 diode array spectrophotometer. EPR spectra were obtained using a Bruker EMX spectrometer, ER 041 XG microwave bridge, and ER 4102ST cavity; samples were run at 77 K in a finger dewar. Room-temperature CD and low-temperature (5 K) MCD spectra in the UV−visible region were collected with a Jasco J-810-150S spectropolarimeter operating with an S-20 photomultiplier tube and an Oxford SM4000-8T magnet. CD and MCD spectra in the near-IR region were obtained with a Jasco J-200-D spectropolarimeter, using a liquid nitrogen cooled InSb detector, and an Oxford SM4000-7T magnet. CD samples were run in a 0.5 cm quartz cuvette. MCD samples were run in cells fitted with quartz disks and a 3 mm rubber spacer. Stopped-flow absorption kinetics with ∼100 ms dead time were obtained using an Applied Photophysics RX2000 mixer, and absorption spectra were recorded using a Hewlett-Packard HP8452A spectrophotometer. Kinetic data with ∼2 ms dead time were obtained using an Applied Photophysics SX.18MV stopped-flow absorption spectrophotometer equipped with a Hg/Xe Arc lamp and outfitted with PEEK tubing. The temperature was maintained using a water/ethanol temperature bath (Fisher Scientific Isotemp 3016).

All oxidized Fet3p samples for spectroscopic characterization were prepared in 100 mM deuterated potassium phosphate buffer with a pD of 7.5, and with 50% (v/v) buffer/glycerol-d_3 (to obtain an optical-quality glass upon freezing). Addition of glycerol had no effect on the Cu sites, as assessed by EPR and absorption spectra.

Reduction potentials of the T1 Cu were obtained by the poised potential method. A 200 μL sample of ∼0.1 mM degassed protein in phosphate buffer pH 6.5 was placed in a 1 cm path length anaerobic cuvette with a Teflon stopcock, and degassed $K_3[Fe(CN)_6]$ was added to yield a final concentration of ∼5 mM. Aliquots of degassed $K_3[Fe(CN)_6]$ were added, and absorption at 608 nm was monitored at room temperature over time until equilibrium was achieved for each titration point (15−20 min).

All stopped-flow kinetic experiments were performed in 100 mM phosphate buffer pH 6.5, and the final protein concentration was 35 μM. The cell path length was 1 cm. For both stopped-flow systems, the tubing, plungers, and valves were made anaerobic by washing with dithionite solution followed by several washes with degassed water or buffer. O_2 inclusion was prevented by a stream of N_2 gas through the system. Kinetic experiments with hydroquinone were performed at 25 °C, and those with Fe(II) were performed at 4 °C.

For Fe(II) spectroscopic measurements, the protein samples were prepared in either deuterated MES buffer with a pD of 6.5 or deuterated potassium phosphate buffer with a pD of 7.0 (for hCp), with 50−60% (v/v) buffer/glycerol-d_3 (to obtain an optical-quality glass upon freezing). To suppress the intense spectroscopic features from the Cu(II) sites, prevent reaction with Fe(II), and be able to observe the weak spectroscopic features from Fe(II), the protein samples were fully reduced prior to Fe(II) addition. Full reduction of Cu sites was achieved by reacting degassed protein samples with 10 equiv (for Fet3 proteins) or 35 equiv (for hCp) of ascorbate for 1−2 h and was confirmed by EPR. For hCp samples, excess ascorbate was removed by washing the protein with deoxygenated buffer using a microcon concentration device (50 000 MW cutoff, Amicon, Inc.) and a VWR Scientific model-V microcentrifuge. All sample manipulations were done in a Vacuum Atmospheres Nexus-1 anaerobic glovebox. The final protein concentration was 0.8−1 mM, and the ascorbate concentration was ∼1−10 mM. Control samples with no protein were prepared with either deuterated MES buffer with a pD of 6.5 or deuterated potassium phosphate buffer with a pD of 7.0, containing 10 mM ascorbate and 50−60% (v/v) buffer/glycerol-d_3. Ferrous MCD samples were loaded under N_2 into cells fitted with Infrasil quartz disks and a 3 mm rubber spacer.

All MCD spectra presented are the subtracted average of the +7 T and −7 T scans (at least 4 scans each), [7 − (−7)]/2 T, to eliminate glass-induced baseline shifts and to increase signal-to-noise ratios. Gaussian fitting of the Fe(II) MCD spectra was performed using PeakFit 4.0 (Jandel). Saturation magnetization data were normalized to the maximum observed intensity and fit according to published procedures to extract ground-state parameters.[69,70]

Calculations of intramolecular electron-transfer (ET) pathways were performed with a multiple pathways program (Harlem) based upon the work primarily of Beratan and Onuchic.[71−75] The crystal structure of hCp was obtained from the Protein Data Bank (1KCW), and the coordinates for the Fet3p model[58] were obtained from Dr. Maria Carmela Bonaccorsi. Protons were added with Insight II or with Harlem.

(62) Calabrese, L.; Mateescu, M. A.; Carbonaro, M.; Mondovi, B. *Biochem. Int.* **1988**, *16*, 199−208.
(63) Reinhammar, B. *Biochim. Biophys. Acta* **1970**, *205*, 35−47.
(64) Reinhammar, B. R. M. *Biochim. Biophys. Acta* **1972**, *275*, 245−259.
(65) Bradford, M. M. *Anal. Biochem.* **1976**, *72*, 248−254.
(66) Goa, J. *Scand. J. Clin. Lab. Invest.* **1957**, *5*, 218−222.
(67) Felsenfeld, G. *Arch. Biochem. Biophys.* **1960**, *87*, 247−251.
(68) Carithers, R. P.; Palmer, G. *J. Biol. Chem.* **1981**, *256*, 7967−7976.
(69) Solomon, E. I.; Pavel, E. G.; Loeb, K. E.; Campochiaro, C. *Coord. Chem. Rev.* **1995**, *144*, 369−460.
(70) Pavel, E. G.; Kitajima, N.; Solomon, E. I. *J. Am. Chem. Soc.* **1998**, *120*, 3949−3962.
(71) Beratan, D. N.; Betts, J. N.; Onuchic, J. N. *Science* **1991**, *252*, 1285−1288.
(72) Beratan, D. N.; Betts, J. N.; Onuchic, J. N. *J. Phys. Chem.* **1992**, *96*, 6, 2852−2855.
(73) Beratan, D. N.; Onuchic, J. N.; Betts, J. N.; Bowler, B. E.; Gray, H. B. *J. Am. Chem. Soc.* **1990**, *112*, 7915−7921.
(74) Beratan, D. N.; Onuchic, J. N.; Hopfield, J. J. *J. Chem. Phys.* **1987**, *86*, 4488−4498.
(75) Onuchic, J. N.; Beratan, D. N. *J. Chem. Phys.* **1990**, *92*, 722−733.

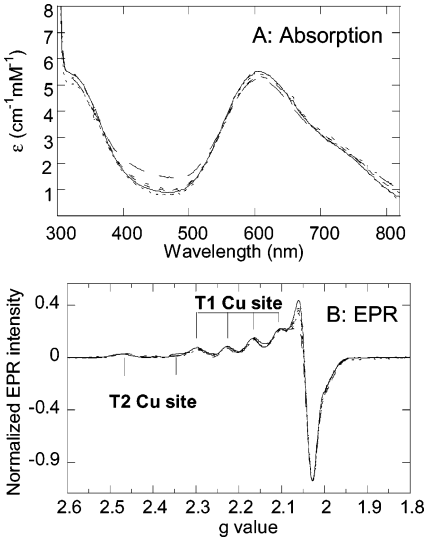

Figure 1. Absorption and EPR of the Fet3 proteins. (A) Absorption spectra at room temperature and (B) EPR spectra at 77 K of Fet3p wt (—), E185A (- - -), E185D (···), Y354A (— —), and Y354F (- - -). EPR spectra were recorded under the following conditions: 9.41 GHz microwave frequency, 10 mW microwave power, 20 G modulation amplitude, 100 kHz modulation frequency, 327 ms time constant, 81.9 ms conversion time. At least 6 scans were averaged to obtain the spectra presented.

Results and Analysis

1. Preparation and Characterization of Fet3p Mutants. The following mutations were generated in Fet3p: E185D, E185A, Y354A, and Y354F. The purified mutated proteins were assayed for protein and Cu concentrations and were spin quantitated by EPR; the results are summarized in Table S1 (Supporting Information). All proteins purified with 4 Cu/protein, with the exception of the E185D and Y354A mutants, which purified with 2.8 Cu/protein. However, the number of spins/protein indicate that 40−50% of the Cu bound to the proteins is paramagnetic, indicating that the Cu is homogeneously loaded into the proteins and that the samples contain some amount of the *apo* form.

The geometric and electronic structure of the Cu sites in the mutants was probed by absorption, circular dichroism (CD), magnetic circular dichroism (MCD), and EPR. For each mutant, the spectra were normalized by the percent of Cu loading indicated in Table S1 to compare to the wild-type protein (wt). The absorption spectrum of wt (Figure 1A) is dominated by two envelopes of intense CT bands: a blue band centered at 608 nm with $\epsilon = 5500\ M^{-1}\ cm^{-1}$, and a shoulder at 330 nm with $\epsilon = 5000\ M^{-1}\ cm^{-1}$, as reported previously.[33] Figure 1 shows that all mutants exhibit the same CT bands, with comparable extinction coefficients. The CD spectrum of wt (Figure S1, Supporting Information) is dominated by ligand field (LF) and CT transitions assigned to the T1 and T3 sites, while the MCD spectrum exhibits LF and CT transitions from the paramagnetic T1 and T2 centers.[33] The CD and MCD spectra of the mutants show no significant difference from those of wt (Figure S1, Supporting Information), indicating that the Cu sites in the mutated proteins have the same LF and CT transitions as wt Fet3p. The EPR spectrum of wt (Figure 1B) shows signals from the T1 and T2 Cu sites, both with $g_{\|} > g_{\perp} > 2.00$, indicative of $d_{x^2-y^2}$ ground states. The T1 Cu signal exhibits a small parallel hyperfine splitting of $A_{\|} = 88 \times 10^{-4}\ cm^{-1}$, and the T2 Cu signal contributes a large parallel hyperfine splitting of $A_{\|} = 190 \times 10^{-4}\ cm^{-1}$, as previously reported.[33,76] The EPR spectra of the mutated proteins (Figure 1B) show no significant difference from that of the wt spectrum. In summary, the spectroscopic characterization of the mutated proteins in comparison to wt Fet3p indicates that the electronic structures of the different Cu sites in these proteins are unaffected by the mutations.

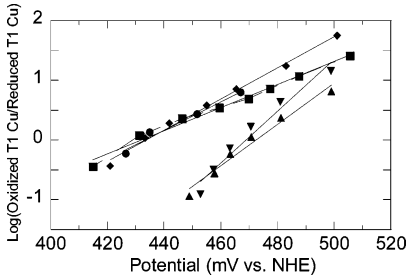

Figure 2. Poised potential titrations of the Fet3 proteins: wt (●), E185A (■), E185D (◆), Y354A (▲), and Y354F (▼). The solid lines are the best fits to the Nernst equation.[77]

2. Thermodynamics and Kinetics. 2.1. Redox Potential of the T1 Cu Site. The reduction potential of the T1 Cu site in the mutated Fet3 proteins was measured by the poised-potential method using the $[Fe(CN)_6]^{3-}/[Fe(CN)_6]^{4-}$ redox couple (Figure 2). The results are summarized in Table 1. In phosphate buffer pH 6.5, the potential of wt is 433 mV, consistent with the previously reported value.[33] The E185 mutants exhibited similar reduction potentials, while the Y354 mutants show an increase of ∼40 mV with respect to wt.

Blue Cu sites exhibit a wide range of redox potentials, and one of the factors that contribute to the potential of these sites is the coordination environment. Overall, four-coordinate blue Cu sites with an axial methionine ligand exhibit a lower range of reduction potentials (240−680 mV) than three-coordinate blue sites (412−1000 mV).[33,78] Mutagenesis studies have shown that the absence of an axial ligand raises the potential of the T1 Cu site by ∼100 mV.[79−81] However, a series of three-coordinate T1 sites in fungal laccases have the same geometric and electronic structure, yet exhibit a wide range of redox potentials (450−790 mV),[82] indicating that the protein matrix plays a major role in tuning the reduction potential of these sites. Fet3p has a three-coordinate blue site, yet its potential is the lowest of any wild-type three-coordinate blue site and is very similar to the potential of the four-coordinate redox-active T1 sites in hCp (448 mV).[33,55] It is evident that the protein matrix in Fet3p lowers the redox potential of its three-coordinate T1 Cu site to be in the same range as the other known multicopper ferroxidase.

(76) Kosman, D. J.; Hassett, R.; Yuan, D. S.; McCracken, J. *J. Am. Chem. Soc.* **1998**, *120*, 4037−4038.
(77) The slopes for the Y354 mutants data differ from those of WT and E185 mutants by about 20 mV. This could reflect reduction of the T1 site in these proteins being a >1 electron process, which is plausible given the presence of other Cu sites in the protein (trinuclear cluster) with redox potentials comparable to that of the T1 Cu site. Alternatively, it can also reflect some protein denaturation during the experiment, which was observed in the Y354 mutants case.
(78) Solomon, E. I.; Szilagyi, R. K.; George, S. D.; Basumallick, L. *Chem. Rev.* **2004**, *104*, 419−458.
(79) Xu, F.; Palmer, A. E.; Yaver, D. S.; Berka, R. M.; Gambetta, G. A.; Brown, S. H.; Solomon, E. I. *J. Biol. Chem.* **1999**, *274*, 12372−12375.
(80) Pascher, T.; Karlsson, B. G.; Nordling, M.; Malmström, B. G.; Vänngård, T. *Eur. J. Biochem.* **1993**, *212*, 289−296.
(81) Hall, J. F.; Kanbi, L. D.; Strange, R. W.; Hasnain, S. S. *Biochemistry* **1999**, *38*, 12675−12680.
(82) Palmer, A. E.; Randall, D. W.; Xu, F.; Solomon, E. I. *J. Am. Chem. Soc.* **1999**, *121*, 7138−7149.

Table 1. Redox Potentials, Rate Constants, Turnover Kinetic Parameters, and Affinity Constants

	T1 redox potential (mV)	second-order rate constant for HQ ($\times 10^6$ M^{-1} s^{-1})	Michaelis–Menton K_M for HQ (mM)[a]	first-order rate constants for Fe(II) (s^{-1})		Michaelis–Menton K_M for Fe(II) (μM)[a]	affinity constants for Fe(II) (M^{-1})
				fast phase	slow phase		
wt	433	0.68 ± 0.07	3.0 ± 0.4	≥ 1200		4.8 ± 1.2	$\geq 1 \times 10^5$
E185D	434	1.32 ± 0.10	8.2 ± 1.1	141 ± 7	2.5 ± 0.4	8.6 ± 1.2	$\geq 1 \times 10^5$
E185A	433	2.62 ± 0.22	14.1 ± 2.3	7.8 ± 0.2	0.8 ± 0.2	40.3 ± 10	$\leq 1 \times 10^2$
Y354A	473	1.70 ± 0.16	4.6 ± 0.8	≥ 1200		16.8 ± 5.3	
Y354F	469	0.58 ± 0.05	12.7 ± 1.6	≥ 1200		5.8 ± 0.5	

[a] Taken from ref 59.

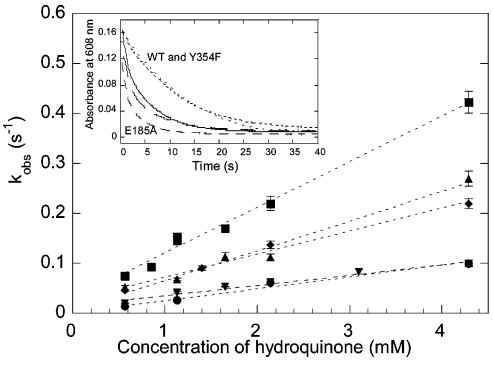

Figure 3. k_{obs} plotted against concentration of hydroquinone for the Fet3 proteins: wt (●), E185A (■), E185D (◆), Y354A (▲), and Y354F (▼). The dotted lines are the least-squares best fits. Inset: representative stopped-flow absorption data for the reduction of the T1 Cu sites of wt (- - -), E185A (— —), E185D (—), Y354A (- —), and Y354F (···) with hydroquinone 4.3 mM. Initial absorption at $t = 0$ was ~0.16.

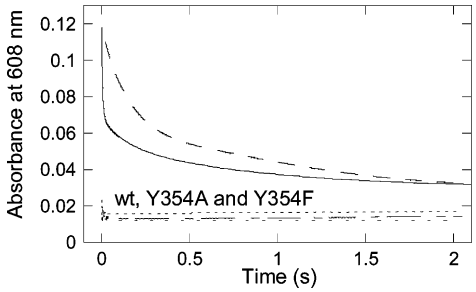

Figure 4. Stopped-flow absorption data of reduction of the T1 Cu sites in Fet3p wt (- - -), E185A (— —), E185D (—), Y354A (- —), and Y354F (···) with 8 equiv of Fe(II). Initial absorption at $t = 0$ was 0.12.

The mutations at the Y354 residues do not change the coordination environment of the blue site in Fet3p; however, replacement of Y354 by either A or F changes the environment around the site enough to raise its potential by ~40 mV. Homology modeling studies of Fet3p, based on the crystal structures of ascorbate oxidase[58] and fungal laccase,[59] position Y354 at about 7 and 9 Å, respectively, from the T1 Cu site, consistent with the observation that this residue modulates the reduction potential of the T1 site.

2.2. Reduction Kinetics of the T1 Cu Site. Reduction of the T1 Cu site of the Fet3 proteins by the bulky organic substrate 1,4-hydroquinone was examined by stopped-flow absorption spectroscopy at 25 °C, in phosphate buffer pH 6.5. Absorption at 608 nm was followed over time after rapid mixing with the reductant. Representative data for the reduction of the mutants by 1,4-hydroquinone (4 mM after mixing) are shown in Figure 3 (inset). For each mutant, the reaction was followed at different concentrations of 1,4-hydroquinone, and the traces were fit with a single-exponential equation to obtain k_{obs}. A plot of k_{obs} against concentration of 1,4-hydroquinone for each mutant is shown in Figure 3; the least-squares fit to these plots yielded the second-order rate constants summarized in Table 1. The second-order rate constant obtained for the reaction with wt is about twice that previously reported,[33] due to a difference in pH (this study was done at pH 6.5, while the first report was done at pH 7.0). Reduction of the Y354F mutant by 1,4-hydroquinone exhibited a second-order rate constant identical to that of wt within experimental error. All other mutations yielded higher rates of reaction with 1,4-hydroquinone: the rates for E185D and Y354A were twice the wt value, while E185A exhibited the highest reaction rate. It is important to note that none of the proteins showed any evidence of saturation behavior up to the maximum 1,4-hydroquinone concentration used (~120-fold excess), indicating that, over the range of concentrations employed, substrate binding is very weak. The reaction of these Fet3 proteins with 1,4-hydroquinone has been previously studied under turnover conditions,[59] and the Michaelis−Menton K_M values are presented in Table 1 for comparison (see Discussion).

Reduction of the T1 Cu site of the Fet3 proteins by Fe(II) was also examined by stopped-flow absorption spectroscopy at 4 °C, in phosphate buffer pH 6.5. Reduction of the T1 Cu site in wt Fet3p by Fe(II) was complete in <2 ms (Figure 4), even at the lowest concentration of Fe(II) used (7−8 equiv). These results show that the reduction of the T1 Cu site in Fet3p by Fe(II) is very fast ($k_{obs} > 1200$ s^{-1}). Previously reported data on the reaction of Fet3p with Fe(II) with an instrument deadtime of 100 ms estimated a $k_{obs} > 23$ s^{-1}.[33] Under the same conditions, reduction of the T1 Cu site in the Y354A and Y354F mutants was also complete within 2 ms (Figure 4), indicating that mutations at the Y354 residue did not have a significant effect on the reaction of Fe(II) with Fet3p within the deadtime of the instrument. In contrast, the E185A and E185D mutants exhibited a slow biphasic reduction of the T1 Cu site (Figure 4). The kinetic traces for the E185A and E185D Fet3 proteins were fit with a double exponential equation, yielding rates of 141 s^{-1} for the fast phase and 2.5 s^{-1} for the slow phase for E185D, and 7.8 and 0.8 s^{-1} for the reaction with E185A, as summarized in Table 1. It is important to note that no biphasic behavior was observed in the reduction kinetics by hydroquinone, as shown in Figure 3 (inset), indicating that the protein samples are homogeneous and the biphasic behavior observed with Fe(II) is intrinsic to this substrate. The results shown in Figure 4 indicate that mutations at the E185 residue lower the reaction rate with Fe(II) and that the depletion of a carboxylate moiety at this position results in the largest decrease in the rate with Fe(II). These observations are consistent with the previously reported trends found in the reaction of these Fet3 proteins with Fe(II) under turnover conditions, where the E185A mutant exhibited the largest increase in K_M (included in Table 1 for comparison).[59,60] The decreased rates of the fast phase correlate

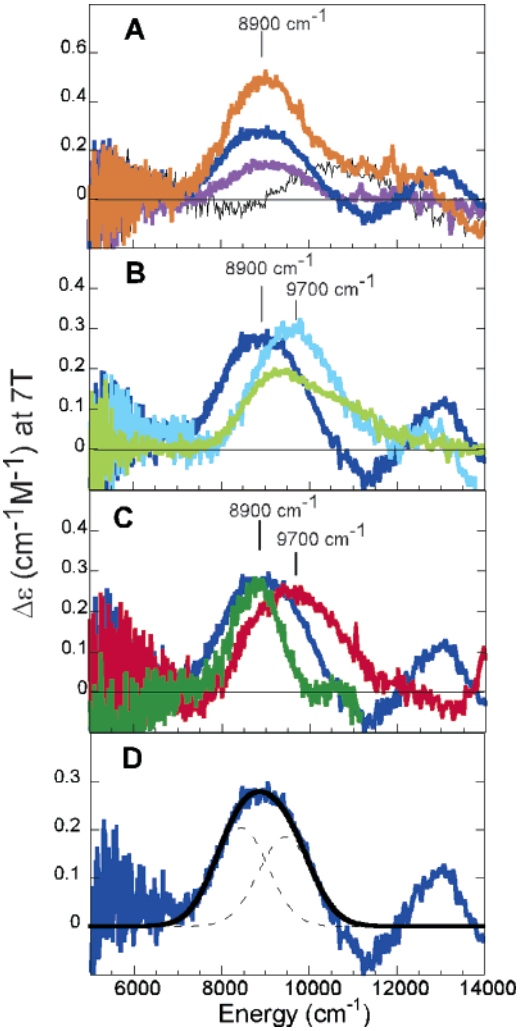

Figure 5. Fe(II) binding to Fet3 proteins. (A) Near-IR MCD spectra of reduced Fet3p wt (black), with 0.5 equiv (purple), 1 equiv (dark blue), and 2 equiv (orange) of Fe(II). (B) Near-IR MCD spectra of reduced Fet3p wt with 1 equiv of Fe(II) in the absence (dark blue) and presence (light blue) of 4 equiv of Zn(II); the MCD spectrum of 1 mM Fe(II) in MES buffer (light green) is shown for comparison. (C) Near-IR MCD spectra of reduced Fet3p wt (dark blue), E185D (dark green), and E185A (red) with 1 equiv of Fe(II). (D) Gaussian fit (black) and components (- - -) of the MCD spectrum of reduced Fet3p wt with 1 equiv of Fe (dark blue).

with the increase in K_M on going from wt to E185D to E185A, while the rate for the slow phase is about the same for both mutants. Therefore, the slow phases have been associated with reduction of the T1 Cu site by Fe(II) nonspecifically bound to the protein, which is expected to yield very slow ET rates.

The dramatic increase in the K_M value for Fe(II) (i.e., decrease in affinity) upon removal of the carboxylate moiety at the E185 position has been interpreted in terms of this residue constituting part of the binding site for Fe(II). To investigate the nature of this putative Fe binding site in Fet3p, the following spectroscopic studies were performed.

3. VTVH MCD Characterization of the Fe(II) Binding Sites in Fet3p: Comparison to hCp. 3.1. Fe(II) Binding to Fet3p. To probe Fe(II) binding to Fet3p, titration of fully reduced protein with ferrous ammonium sulfate was followed by MCD (Figure 5A) in the near-IR region, where non heme Fe(II) sites exhibit LF transitions.[83] A signal at ~8900 cm^{-1} grows upon addition of 0.5 (purple spectrum) and 1 (blue) equiv of Fe(II). The spectrum at 2 equiv (orange) of Fe(II) also shows intensity at around 9700 cm^{-1}, where free Fe(II) in solution absorbs (Figure 5B, light green spectrum). The intensity at 9700 cm^{-1} in the spectrum of the 2 equiv of Fe(II) sample quantitates to ~1 equiv of unbound Fe(II), indicating that no more than 1 equiv of Fe(II) binds to Fet3p. Following the intensity at ~8900 cm^{-1}, an affinity constant for Fe(II) to Fet3p of at least 1×10^5 M^{-1} can be estimated. Fully reduced wt protein with 1 equiv of Fe(II) in the presence of 4 equiv of zinc nitrate does not show intensity at ~8900 cm^{-1} (Figure 5B, light blue); instead, it exhibits a signal at ~9700 cm^{-1}, characteristic of free Fe(II) in solution (light green). These results indicate that Zn(II) binds to the iron binding site and prevents Fe(II) from binding to Fet3p. Turnover kinetic experiments have shown that Zn(II) inhibits ferroxidase activity in Fet3p, consistent with the above results that Zn(II) competes for the Fe(II) binding site in Fet3p. These observations further support the assignment of the signal at ~8900 cm^{-1} as Fe(II) bound to the substrate binding site in Fet3p.

The mutated Fet3 proteins were titrated with Fe(II) in a similar manner. The MCD spectrum of fully reduced E185D with 1 equiv of Fe(II) also exhibits a signal at ~8900 cm^{-1} (Figure 5C, dark green). The E185D spectrum shows no intensity in the region where free Fe(II) absorbs, indicating that 1 equiv of Fe(II) is fully bound to the protein. A lower limit to the affinity constant of E185D for Fe(II) is estimated to be $\geq 1 \times 10^5$ M^{-1}, based on the detection limit of the experiment. The spectrum of Fe(II) bound to E185D (Figure 5C, dark green) is somewhat different in line shape (sharper) as compared to the spectrum of Fe(II) bound to wt (Figure 5C, blue), probably due to differences in geometry and metal−ligand distances associated with having a shorter residue as a ligand (aspartate vs glutamate). In contrast, reduced E185A with 1 equiv of Fe(II) exhibits a signal at ~9700 cm^{-1} (red), around the same energy as free Fe(II) in solution (Figure 5B, light green). The E185A spectrum shows no intensity in the region where Fe(II) bound to Fet3p absorbs, indicating that the 1 equiv of Fe(II) added is mostly free in solution. An upper limit of $\leq 1 \times 10^2$ M^{-1} can be estimated for the affinity constant of Fe(II) for E185A. These results are consistent with turnover kinetic experiments that have shown E185A to exhibit a major increase in K_M.[59,60] The K_M values for Fe(II) from one of these studies are listed in Table 1, along with the estimates for the affinity constants from the binding titrations in this study.

The Gaussian resolution of the signal from Fe(II) bound to Fet3p is presented in Figure 5D and reveals two bands at 8400 and 9500 cm^{-1}. It is important to note that no signals are observed in the low energy region of the spectrum. The study of a series of non heme Fe(II) sites with different geometries has demonstrated that the splitting of the ^5E_g excited state ($\Delta^5E_g \equiv d_{x^2-y^2} - d_{z^2}$) is sensitive to the coordination number and geometry of the Fe(II) site.[70,83] Near-IR MCD spectroscopy allows the direct observation of these d → d transitions. In general, six-coordinate distorted octahedral ferrous sites show two transitions centered at ~10 000 cm^{-1}, split by <2000 cm^{-1}; five-coordinate sites show two transitions at ~10 000 and ~5000 cm^{-1}, which shift to lower energy on going from a square pyramidal to a trigonal bipyramidal ligand field; and distorted

(83) Solomon, E. I.; Brunold, T. C.; Davis, M. I.; Kemsley, J. N.; Lee, S.-K.; Lehnert, N.; Neese, F.; Skulan, A. J.; Yang, Y.-S.; Zhou, J. *Chem. Rev.* **2000**, *100*, 235−349.

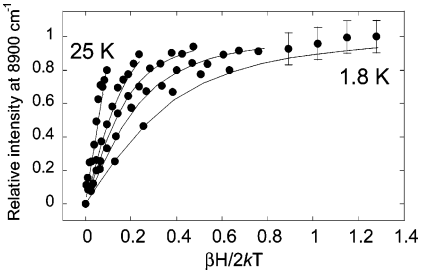

Figure 6. VTVH saturation data on the reduced Fet3p wt sample with 1 equiv of Fe(II). Data were taken at 8700 cm^{-1}, fixed temperatures of 1.8, 3, 5, 10, and 25 K, and a series of fixed fields. Representative error bars (averaged over several data sets) are shown. Fits to the data using the parameters described in the text are drawn with solid black lines.

four-coordinate sites show only low energy transitions, in the region of 4000−7000 cm^{-1}. According to these trends in excited-state splitting, the spectrum in Figure 5D associated with Fe(II) bound to Fet3p reflects a six-coordinate distorted octahedral site, with a 10Dq of 8850 cm^{-1} and a Δ^5E_g of ∼1100 cm^{-1}.

The MCD signal at 8900 cm^{-1} associated with Fe(II) bound to Fet3p saturates at high field and low temperature; the saturation data are shown in Figure 6. The temperature and field dependences of an MCD transition are characterized by the nesting (nonsuperimposing behavior) of isotherms when the MCD intensity is plotted against $\beta H/2kT$ (as in Figure 6); this nesting behavior can be used to gain insight into the ground-state electronic structure of the Fe(II) site.[69,83] To obtain ground-state parameters associated with the zero-field splitting (ZFS) of an $S = 2$ high-spin ferrous site, the experimental saturation behavior can be computationally fit to an orientation-averaged intensity expression that includes the rhombic ZFS (given by δ) and the Zeeman splitting (given by $g_{||}$) of the non-Kramers $M_s = \pm 2$ doublet, as well as the transition polarization ratio (M_z/M_{xy}) and contributions from linear temperature-independent B-terms and low-lying excited states. The ground-state parameters δ and $g_{||}$ are directly related to the splitting of the $^5T_{2g}$ ground state; thus the dπ orbital splittings $\Delta \equiv d_{xz,yz} - d_{xy}$ and $V \equiv d_{xz} - d_{yz}$ may be determined. The best fit to the saturation data for Fe(II) bound to Fet3p is achieved with $\delta = 6.7$ cm^{-1} and $g_{||} = 8.2$ (fit shown in Figure 6); however, due to the very low signal intensity, large error bars are associated with the data, which can be fit with a range of δ and $g_{||}$ values. Therefore, within experimental error (representative error bars are shown in Figure 6), the ground-state parameters for Fe(II) bound to Fet3p are as follows: $4.5 < \delta < 7$ cm^{-1} and $8.0 < g_{||} < 9.2$. A ZFS $\delta > 4.5$ cm^{-1} corresponds to an orbital splitting of $-\Delta < 400$ cm^{-1} and a ratio of $|V/2\Delta| > 0.2$, close to the rhombic limit. For a $|V/2\Delta| > 0.2$ and a $g_{||} < 9.2$, $-\Delta$ must quite small, that is, ∼200 cm^{-1}. These ground-state parameters are consistent with the substrate Fe(II) bound to Fet3p having a six-coordinate structure.

3.2. Comparison to hCp. To probe Fe(II) binding to hCp and compare it to Fet3p, fully reduced hCp was also titrated with ferrous ammonium sulfate and followed by MCD (Figure 7A) in the near-IR region. A signal at ∼8900 cm^{-1} grows upon addition of 0.5 (purple) and 1 (blue) equiv of Fe(II). The spectra at 2 (orange) and 4 (dark green) equiv of Fe(II) also exhibit intensity at lower energy (<8500 cm^{-1}), where free Fe(II) in solution absorbs (Figure 7B, light green). Following the intensity at ∼8900 cm^{-1}, an affinity constant of at least 1×10^5 M^{-1} can be estimated, consistent with the previously reported value from an equilibrium dialysis study.[84] Two Fe(II) binding sites have been identified from the crystal structure of hCp.[45] The characterization of the second binding site is potentially obscured by the MCD intensity of Fe(II) in solution at low energy in phosphate buffer (Figure 7B, light green). A titration of reduced hCp with ferrous ammonium sulfate in MES buffer (Figure S2, Supporting Information) allowed a further characterization of the Fe(II) binding sites, because Fe(II) in MES buffer solution has all MCD intensity at >8500 cm^{-1}. Figure S2 shows no new bands growing at low energy, indicating that Fe(II) binding to both sites contributes MCD intensity only in the 8900 cm^{-1} region. Titration of fully reduced hCp protein with 1 equiv of Fe(II) in the presence of 4 equiv of zinc nitrate exhibits broad absorption at low energy (Figure 7B, light blue), where free Fe(II) (in phosphate solution) absorbs (light green). Kinetic studies have demonstrated that Zn(II) exhibits competitive inhibition of ferroxidase activity in hCp, and an affinity constant of 3×10^5 M^{-1} for Zn(II) has been reported.[84] Our MCD results indicate that Zn(II) binding prevents Fe(II) from binding to the protein and confirm the assignment of the 8900 cm^{-1} signal (Figure 7B, dark blue) as Fe(II) bound to hCp.

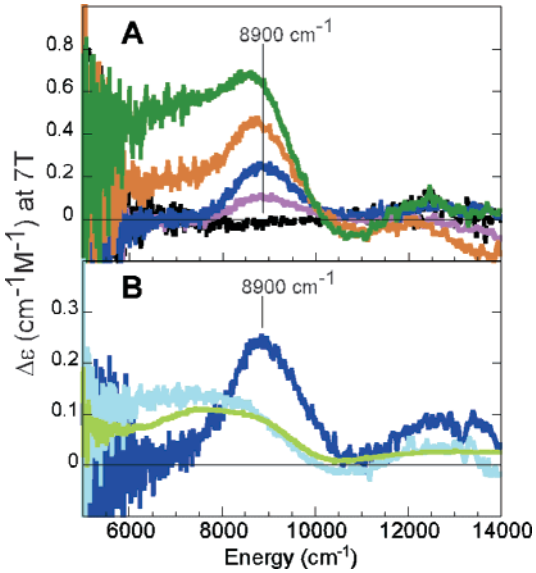

Figure 7. Fe(II) binding to hCp in phosphate buffer. (A) Near-IR MCD spectra of reduced hCp (black), with 0.5 equiv (purple), 1 equiv (dark blue), 2 equiv (orange), and 4 equiv (dark green) of Fe(II). (B) Near-IR MCD spectra of reduced hCp with 1 equiv of Fe(II) in the absence (dark blue) and presence (light blue) of 4 equiv of Zn(II); the MCD spectrum of 1 mM Fe(II) in phosphate buffer (light green) is shown for comparison.

Figure 8A shows a comparison of the MCD spectra of Fe(II) bound to Fet3p and hCp. The signal from Fe(II) bound to hCp is sharper than the one from Fe(II) bound to Fet3p and can be fit with either one or two Gaussian bands (Figure S3 in Supporting Information). However, the VTVH MCD saturation magnetization behavior of this signal is almost identical to that of Fe(II) bound to Fet3p (Figure 8B, blue is hCp, red is Fet3p), and its analysis also yields a large ZFS ($4.5 < \delta < 7$ cm^{-1}) and $g_{||}$ of 7.5−8.5. As discussed above, ground-state parameters of these magnitudes indicate the presence of a small $^5T_{2g}$ ground-state splitting, and thus a six-coordinate site with rhombic distortion. Therefore, the signal from Fe(II) bound to hCp was

(84) McKee, D. J.; Frieden, E. *Biochemistry* **1971**, *10*, 3880−3883.

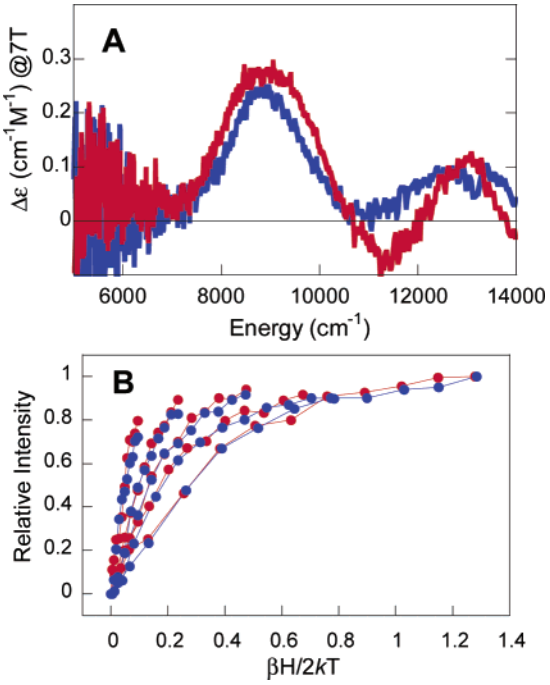

Figure 8. Comparison of Fe(II) bound to hCp and Fet3p. (A) Near-IR MCD spectra of reduced hCp (blue) and reduced Fet3p (red) with 1 equiv of Fe(II). (B) VTVH saturation data (●) on the hCp (blue) and Fet3p (red) signals. Data were taken at 8700 cm^{-1}, fixed temperatures of 1.8, 3, 5, 10, and 25 K, and a series of fixed fields.

resolved with two Gaussian bands at 8700 and 9600 cm^{-1}, resulting in a 10Dq of 9150 cm^{-1} and a Δ^5E_g of ~900 cm^{-1}, similar to Fet3p.

In summary, Fe(II) binds to Fet3p and hCp with high affinity, and the Fe(II) binding sites in these proteins are best described as six-coordinate distorted octahedral sites. For comparison, 1 equiv of Fe(II) was added to fully reduced laccase, a multicopper oxidase that does not exhibit specificity for Fe(II).[33] In contrast to Fet3p and hCp, the near-IR MCD spectrum of reduced laccase with Fe(II) shows a signal at ~9600 cm^{-1}, around the same energy as free Fe(II) in solution (Figure S4, Supporting Information), indicating that this multicopper oxidase does not exhibit high affinity binding of Fe(II).

Discussion

We have examined the reactivity of the T1 Cu sites of a series of Fet3p mutants with two classes of substrate: 1,4-hydroquinone, a bulky organic substrate, and Fe(II), which is the specific substrate of this enzyme. These two substrates exhibit large differences in affinities for the protein: 1,4-hydroquinone has weak binding, while Fe(II) exhibits high affinity binding for Fet3p. Our discussion first focuses on the interpretation of the reactivity of these proteins toward 1,4-hydroquinone in terms of the semiclassical theory for intermolecular electron transfer (ET) to calibrate the analysis. A discussion of the nature of the binding site for Fe(II) in Fet3p follows, and the contribution of this binding site to ferroxidase activity will be analyzed. Finally, the factors that control ET from the protein-bound Fe(II) substrate to the T1 Cu site will be discussed.

Electron Transfer from 1,4-Hydroquinone to the T1 Cu Site. According to the semiclassical theory for intermolecular ET,[85] the rate of ET from 1,4-hydroquinone to the T1 Cu site, k_{ET}, is dependent upon the following factors: the steric term (S), the equilibrium constant for formation of the interaction complex between the donor and the acceptor (K_A), the electronic coupling matrix element (H_{DA}), the driving force ($\Delta G°$), and the reorganization energy (λ), as indicated in eq 1.

$$k_{ET} = SK_A(4\pi^3/h^2\lambda kT)^{1/2}(H_{DA})^2 \exp[-(\Delta G° + \lambda)^2/4\lambda kT] \quad (1)$$

The reorganization energy of the T1 Cu sites is the same for all of the Fet3p mutants studied, given that the geometric and electronic structure of the T1 site was unaffected by the mutations. The reduction potentials of the T1 Cu sites increased by ~40 mV for the Y354 mutations (see Table 1). Therefore, the driving force for the reaction of these mutants with 1,4-hydroquinone would be ~1 kcal/mol greater than that for the reaction of wt, and a 2-fold increase is predicted for the rate of reaction. The second-order rate constant for Y354A Fet3p is indeed about double the rate of wt Fet3p (Table 1); however, the rate constant for the Y354F protein is about the same as that for wt Fet3p. Thus, the other factors to consider are S and K_A, which are related to the affinity constant for the substrate. Although there is no direct measurement of the magnitude of the affinity of the Fet3 proteins for 1,4-hydroquinone, the Michaelis−Menton constants (K_M) determined from turnover kinetic experiments[59] give the qualitative trend. The Y354A mutant showed a K_M for 1,4-hydroquinone very similar to that of wt Fet3p, while for the Y354F mutant there is a significant increase (see Table 1). The K_M increase for the Y354F mutant predicts a decrease in the SK_A term, which would decrease the rate of ET to the T1 Cu site in this mutant relative to wt. Thus, while the increased rate of reaction with 1,4-hydroquinone observed for the Y354A mutant can be explained mainly by the increase in reduction potential of the T1 Cu site, the rate of reaction of the Y354F did not change from that of wt, because of two competing factors: an increased reduction potential of the T1 Cu site, and a decreased affinity for 1,4-hydroquinone.

In contrast to the Y354 mutants, the driving force for the reaction of the E185 mutants with 1,4-hydroquinone remained the same as for wt Fet3p. However, the K_M values for the E185 mutants (see Table 1) indicate that their affinities for 1,4-hydroquinone have significantly decreased: E185D exhibits a lower affinity than wt Fet3p, while E185A showed the lowest affinity of all mutants studied. According to eq 1, this trend in affinity for the substrate (SK_A term) predicts the following trend in ET rates: k_{ET} (wt) > k_{ET} (E185D) > k_{ET} (E185A), which is opposite to the observed trend in the second-order rate constants (Table 1). Because the reorganization energy and the driving force are the same for these reactions, the factor that could correlate with the observed trend in rates is the electronic coupling matrix element H_{DA}, which relates to the ET pathways from the 1,4-hydroquinone to the T1 Cu site. It is not possible to quantitatively assess the relative contributions of H_{DA} to k_{ET} in the absence of a crystal structure of Fet3p; however, given the observed trend in k_{ET}, one can infer that H_{DA} (wt) < H_{DA} (E185D) < H_{DA} (E185A). This trend in H_{DA} suggests that the ET pathway from the 1,4-hydroquinone to the T1 Cu site is perturbed in the E185 mutants and becomes more favorable as the size of the mutated residue decreases.

It is important to note that the effects of the E185 mutations on the H_{DA} and overall k_{ET} from 1,4-hydroquinone to the T1

(85) Marcus, R. A.; Sutin, N. *Biochim. Biophys. Acta* **1985**, *811*, 265−322.

Cu site show an opposite trend to that observed for Fe(II) (vide infra). Also, in contrast to the Fe(II) case, the affinity for hydroquinone was only modestly perturbed by the E185A mutation (Table 1). These observations suggest that the substrate site and ET pathways used by 1,4-hydroquinone differ from those used by the Fe(II) substrate.

Nature of the Ferrous Binding Site in Fet3p. Ferrous binding to Fet3p has been probed by a VTVH MCD methodology developed for Fe(II),[70,83] and the spectroscopic features of Fe(II) bound to this protein have been identified using a combination of site-directed mutagenesis and zinc competition for the binding site. The estimates for the affinity constants for Fe(II) obtained from MCD indicate that the E185 residue must be part of the binding site for Fe(II), as suggested by previous mutagenesis studies.[59,60] According to its spectroscopic features and saturation magnetization behavior, Fe(II) bound to Fet3p is a six-coordinate site. This is the first time that the geometric and electronic structure of a substrate bound to a multicopper oxidase has been examined and the contributions of the binding site to the reactivity of the substrate have been analyzed.

The spectroscopic signatures of Fe(II) bound to Fet3p have been correlated to those from Fe(II) bound to hCp, another multicopper ferroxidase for which crystallographic data are available.[43−45] Our spectroscopic analysis indicates that the Fe(II) binding sites in Fet3p and hCp are similar in nature and can be described as distorted six-coordinate. The crystal structures of metal-bound hCp[45] have identified one histidine and three carboxylic amino acids as putative ligating residues. The orientation of the carboxylic residues in each of these sites is such that they are all likely monodentate ligands to the Fe(II). Therefore, the coordination environment for Fe(II) bound to hCp is most reasonably described as having three monodentate carboxylates, one histidine, and two waters. No crystal structure of Fet3p is currently available; however, our spectroscopic comparisons (Figure 8) suggest that a similar coordination environment must be present for Fe(II) bound to Fet3p. Enough evidence has been gathered from the studies described above, as well as sequence homology[58] and site-directed mutagenesis results,[59−61] to assign the E185 residue as one of the ligands for Fe(II). D278 is likely to be one of the other carboxylate ligands, given that D278A shows the second largest decrease in K_M for Fe(II) out of all mutations of carboxylate residues to Ala (E185A is larger).[59] The other two Fet3 protein ligands for Fe(II) remain to be identified.

Electron Transfer from Fe(II) to the T1 Cu Site: Redox Potential of Protein-Bound Iron. The driving force for the reaction of the T1 Cu sites in Fet3p and hCp with Fe(II) must be very large, given that this reaction is stoichiometric. However, the reduction potential of the T1 Cu sites in these proteins is about 430 mV,[33] while the estimated reduction potential of the Fe(II)/Fe(III) couple in aqueous solution is ∼420 mV at pH 6.5.[86] Therefore, the reactive Fe(II) species cannot be free Fe(II) in solution, and the Fe(II) binding site in these proteins must play an important role in modulating the redox potential of the Fe(II)/Fe(III) couple bound to the protein. Given the reduction potential of the T1 Cu sites in Fet3p and hCp (∼430 mV), the potential of protein-bound Fe should be ≤190 mV (at least 240 mV lower than the T1 Cu site) for the reaction to be stoichiometric. The protein modulates the relative affinities for Fe(II) and Fe(III) to achieve such low redox potential. Our MCD titration studies have shown that the affinities of hCp and Fet3p for Fe(II) are at least 10^5 M^{-1}; therefore, the affinity of these proteins for Fe(III) should be at least 10^{15} M^{-1} for the redox potential of protein-bound Fe to be ∼190 mV.[87] Alternatively, to ensure efficient product release, the affinity of the multicopper ferroxidases for Fe(III) should not exceed that of the protein to which this metal ion is transferred under physiological conditions. In the case of hCp, the crystal structure reveals a negatively charged patch situated above each of the Fe(II) binding sites.[45] This negative patch is believed to be a trivalent metal ion binding site that serves as a short term holding site for Fe(III) shuttling to transferrin, the ultimate Fe(III) acceptor in plasma. Transferrin exhibits an affinity for Fe(III) of $\sim 10^{20}$ M^{-1};[88] therefore, the affinity of hCp for Fe(III) should not exceed $\sim 10^{16}$ to allow effective trafficking of this ion to the Fe(III) holding sites and finally to transferrin. This latter value sets a lower limit for the reduction potential of Fe bound to hCp at ∼120 mV. A different scenario exists for Fet3p, which forms a specific enzyme complex with Ftr1p, the iron permease that transports Fe(III) across the membrane.[39] It has been demonstrated that an association of Fet3p with Ftr1p is necessary for the transfer of Fe(III) from Fet3p to the latter and that only Fe(III) generated through the ferroxidase reaction of Fet3p can be transported across the membrane by Ftr1p. It is possible that a "holding" site for Fe(III) is formed upon association of these proteins to facilitate the transfer of Fe(III). However, little is known about the mechanism of such a transfer or the affinity of the Fet3p/Ftr1p complex for Fe(III). In summary, the Fe binding sites in Fet3p and hCp modulate the relative affinities for Fe(II) and Fe(III) to lower the reduction potential to at least 190 mV, while keeping the affinity for Fe(III) in a reasonable range to ensure effective trafficking of Fe(III).

One of the factors that controls the relative affinities of a site for the oxidized and reduced metal ion is the coordination environment. For iron bound to hCp or Fet3p to exhibit a reduction potential of ∼190 mV, the ratio of the affinities of these proteins for Fe(III) and Fe(II) must be $\sim 10^{10}$. Overall, oxygen donor ligands stabilize Fe(III) more than Fe(II); comparing the stability constants of dicarboxylic ligands for Fe(III) and Fe(II), one finds that their affinity for Fe(III) can be 4−10 orders of magnitude higher than that for Fe(II). In contrast, nitrogen donor ligands tend to stabilize Fe(II) more than Fe(III). As discussed above, the coordination environment of iron bound to Fet3p and hCp is likely composed of three monodentate carboxylates, one histidine, and two waters, that is, mostly oxygen donor ligands. The presence of at least one nitrogen donor is important to keep a high affinity for Fe(II), while the set of oxygen donor ligands allows the protein to have an even higher affinity for Fe(III). Comparatively, the coordination environment in ferric binding proteins, like human transferrin and its bacterial homologues (e.g., nFbp), is composed of one histidine, one carboxylate, two tyrosines, and one exogenous

(86) The standard reduction potential for the Fe(II)/Fe(III) couple in aqueous solution is +770 mV. The redox potential at pH 6.5 was calculated using the stability constants for the relevant iron hydroxide complexes at this pH range, taken from the Pourvaix diagrams.

(87) From a thermodynamic cycle that includes the oxidation of Fe(II) bound to the protein, the affinities of the protein for Fe(II) and Fe(III), and the oxidation of aqueous Fe(II), the following equation may be derived: $E_{aq}^{\circ} - E_{protein-bound}^{\circ} = 59 \log(\beta_{III}/\beta_{II})$, which relates the reduction potential of the protein-bound Fe to the reduction potential of aqueous iron and the affinities of the protein for Fe(III) and Fe(II), β_{III} and β_{II}, respectively.

(88) Aisen, P.; Leibman, A.; Zweier, J. *J. Biol. Chem.* **1978**, *253*, 1930−1937.

anion, carbonate, phosphate, citrate, or oxalate.[89,90] In these proteins, high affinity for Fe(III) is also achieved by using oxygen donor ligands and by neutralizing the metal charge with negatively charged residues. However, the presence of tyrosine ligands tend to stabilize the Fe(III) complex even more than the sites in Fet3p and hCp. The bacterial and human transferrins exhibit even higher ratio of affinities for Fe(III) and Fe(II) ($10^{17}-10^{20}$), and the reduction potentials of these sites are in the range of -200 to -500 mV.[91,92]

Another factor that contributes to the reduction potential of metal sites in proteins is the dielectric constant of the protein environment, which is significantly lower (4−15) than that of aqueous environment (78.5). A low dielectric environment will contribute to the redox potential by destabilizing higher charges. In the case of iron bound to Fet3p or hCp, the protein provides three negatively charged carboxylate ligands, the charge of the reduced species is −1, and the charge of the Fe(III) species is zero (i.e., $[Fe(H_2O)_2His(COO^-)_3]^0/[Fe(H_2O)_2His(COO^-)_3]^{-1}$), in contrast to iron in aqueous solution where the charge of the reduced species at pH 6.5 is 2+ and that of the oxidized species is 1+ (i.e., $[Fe(H_2O)_4(HO^-)_2]^+/Fe(H_2O)_6^{2+}$). In both cases, the net charge of the reduced species is higher than that of the oxidized species, and a decrease in dielectric constant is expected to decrease their reduction potentials. According to the Born model, the electrostatic contribution to the free energy of solvation (ΔG_{solv}) is given by $(1 - \epsilon)q^2/2\epsilon R$, where ϵ is the relative dielectric constant of the medium with respect to vacuum, q is the charge, and R is the radius of the solvated species. Because the magnitude of ΔG_{solv} is proportional to the square of the charge, the ΔG_{solv} for iron in solution at pH 6.5 will be larger than that of iron bound to Fet3p and hCp. Thus, these proteins also reduce the contribution of the ΔG_{solv} term to the reduction potential (as compared to aqueous iron) by providing negatively charged residues that reduce the net charges of the redox couple.

In summary, the iron binding sites in Fet3p and hCp play a major role in tuning the substrate ligation to modulate the reduction potential of protein-bound Fe(II) and provide a large driving force for the ferroxidase reaction. Two main factors contribute to the modulation of the reduction potential of protein-bound iron: the ligand set and the lower dielectric constant provided by the protein.

Electron Transfer from Fe(II) to the T1 Cu Site: ET Pathways. The rate of ET from protein-bound Fe(II) to the T1 Cu site is dependent upon the factors indicated in eq 1. The reaction of Fe(II) with Fet3p slowed significantly when the E185 residue was mutated: the reaction rate for E185D is at least 8× slower than wt, while that for E185A is at least 150× slower with respect to wt (Table 1).[93] The two main factors that likely correlate with this trend are the SK_A and H_{DA} terms, given that the reorganization energy and the reduction potential of the T1 Cu sites in these mutants are the same as in wt. In our MCD titrations, the same lower limit for the stability constant of the Fe(II)−protein complex was obtained for E185D and wt, while the affinity of E185A for Fe(II) is estimated to be at least 1000× lower (Table 1). This loss in affinity for Fe(II) (decrease in SK_A term) is large enough to explain the decreased rate of the E185A mutant. Therefore, the slow reduction of the T1 Cu site observed for this mutant is mostly due to ET from Fe(II) nonspecifically bound to the protein. In the case of E185D, no apparent loss of affinity for Fe(II) was observed; thus, the decreased reaction rate must be related to a decrease in the H_{DA} term.

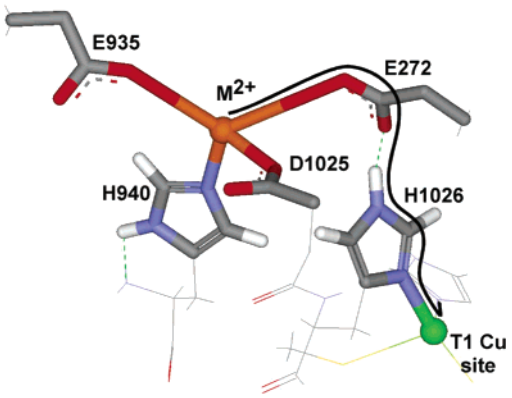

Figure 9. Divalent metal ion binding site in hCp. The putative ligating residues are E935, E272, H940, and D1025. The most efficient ET pathway to the T1 Cu site is indicated with the black arrow. Figure generated from the crystal structure of hCp (ref 45, PDB accession number 1KCW).

Table 2. Electron-Transfer Pathways to the T1 Cu Site

	decay coupling	calcd β (Å^{-1})[a]	relative k_{ET}
E272 pathway	0.028	1.19	12
D1025 pathway	0.008	1.61	1
H940 pathway	0.0019	2.09	0.06

[a] Using a donor−acceptor distance of 8.9 Å.

The relative contribution of H_{DA} to k_{ET} can be analyzed by identifying the best intramolecular ET pathways from the protein-bound Fe(II) to the T1 Cu site, using a program developed by Beratan and Onuchic.[71−75] For a given pathway, H_{DA} is proportional to the product of decay factors associated with the covalent bonds, hydrogen bonds, and space jumps along the pathway. Using the crystal structure of hCp,[45] the ET pathways from the divalent metal binding site to the T1 Cu site in domain 6 have been evaluated.[55] The ligands for Fe(II) are E272, D1025, E935, and H940 (see Figure 9), and three main ET pathways have been identified; the decay couplings and β values associated with these pathways are listed in Table 2. The best ET pathway is through the liganding Oϵ2 of the E272 residue, to the other carboxylate oxygen, which is hydrogen bonded to the Nϵ2 of H1026, a ligand of the T1 Cu site. The next best pathway is through the Oδ2 of D1025, through a space jump to the Cδ2 of H1026. The third pathway goes through the Nϵ2 and Cδ2 of H940, then through a space jump to the Cδ2 of H1026. All pathways go into the T1 Cu site through its H1026 ligand; however, the E272 pathway goes through the remote nitrogen of the histidine, while the other two couple into the Cδ2. A W-band ENDOR study[94] on ^{15}N-enriched single crystals of azurin has detected spin density at the remote nitrogens of the T1 Cu site histidine ligands (~0.25% of the

(89) MacGillivray, R.; Moore, S.; Chen, J.; Anderson, B.; Baker, H.; Luo, Y.; Bewley, M.; Smith, C.; Murphy, M.; Wang, Y.; Mason, A.; Woodworth, R.; Brayer, G.; Baker, E. *Biochemistry* **1998**, *37*, 7919−7928.
(90) Shouldice, S.; Dougan, D.; Skene, R.; Tari, L.; McRee, D.; Yu, R.; Schryvers, A. *J. Biol. Chem.* **2003**, *278*, 11513−11519.
(91) Taboy, C.; Vaughan, K.; Mietzner, T.; Aisen, P.; Crumbliss, A. *J. Biol. Chem.* **2001**, *276*, 2719−2724.
(92) Dhungana, S.; Taboy, C.; Anderson, D.; Vaughan, K.; Aisen, P.; Mietzner, T.; Crumbliss, A. *Proc. Natl. Acad. Sci. U.S.A.* **2003**, *100*, 3659−3664.
(93) This trend refers to the rate constant for the fast phase.
(94) Coremans, J. W. A.; Poluektov, O. G.; Groenen, E. J. J.; Canters, G. W.; Nar, H.; Messerschmidt, A. *J. Am. Chem. Soc.* **1996**, *118*, 12141−12153.

total spin density). Thus, the E272 pathway is most efficient, not only because it involves a direct hydrogen bond to a ligand of the T1 Cu site, but also because it couples into an atom that contributes to the total spin density of the ground state of the electron acceptor. The relative contributions of the three ET pathways to k_{ET} can be evaluated by comparing the ratios of the decay coupling squared. The contribution of the E272 pathway to k_{ET} is $\sim 10\times$ larger than that of the next best pathway (through D1025), and $200\times$ larger than the H940 pathway (Table 2).

In the absence of a crystal structure for Fet3p, it is not possible to do an ET pathway analysis as that described for hCp. However, two models have been constructed for Fet3p on the basis of its homology modeling.[58,59] They both place the E185 residue in the vicinity of the T1 Cu site, and one of them[58] places E185 in an analogous position to the E272 residue in hCp. If this is the case, a mutation of E185 in Fet3p is expected to disturb the interaction of this residue with the histidine ligand to the T1 Cu site (H489). In the case of E185D, because aspartate is one carbon atom shorter than glutamate, the relative position of the carboxylate moiety to the remote nitrogen of H489 would not be favorable for hydrogen bonding and the efficiency of the pathway would significantly decrease. Thus, the decrease in reaction rate with Fe(II) observed for the E185D mutant can be explained in terms of disruption of the most efficient ET pathway to the T1 Cu site (Figure 9). The next best pathway is $\sim 10\times$ slower, which is consistent with the decrease observed in the reaction rate of E185D with Fe(II) (Table 1) with respect to wt Fet3p.

In summary, the dramatic decrease in the reaction rate with Fe(II) effected by the E185A mutation can be attributed mainly to its loss of affinity for Fe(II), while the moderate decrease in rate observed for the E185D mutant can be explained in terms of the loss of the most efficient ET pathway to the T1 Cu site. The effect of the E185D mutation is quite interesting in that it disrupts the best ET pathway to the T1 Cu site, while maintaining a high affinity for the Fe(II) substrate. The study of the E185A and E185D mutations has allowed the resolution of the two main roles that the E185 residue plays in ferroxidase activity: as a ligand for Fe binding and as part of the most efficient ET pathway to the T1 Cu site.

Acknowledgment. We thank the Stanford Blood Center for providing human plasma, Drs. Timothy Machonkin and Serena DeBeer-George for helpful discussions on ET pathways, Drs. David Beratan, Jeff Regan, and Igor Kunikov for providing the ET pathway analysis program, and Dr. Maria Carmela Bonaccorsi di Patti for providing the coordinates for the Fet3p model. This research was supported by NIH Grants DK31450 (for E.I.S.) and DK53820 (for D.J.K.).

Supporting Information Available: Information on protein characterization (Table S1), CD and MCD spectra of the Fet3p mutants, near-IR MCD spectra of reduced hCp titrated with Fe(II) in MES buffer, Gaussian fits of the MCD spectrum of Fe(II) bound to hCp, and comparison of the near-IR MCD spectra of reduced Fet3p and reduced laccase with 1 equiv of Fe(II). This material is available free of charge via the Internet at http://pubs.acs.org.

JA049220T